Supplementary figures

Title: A Deep Learning Integrated Radiomics Model for Identification of Coronavirus Disease 2019 Using Computed Tomography

Authors: Xiaoguo Zhang[1§], Dawei Wang[2§], Jiang Shao[3], Song Tian[2], Weixiong Tan[2], Yan Ma[1], Qingnan Xu[1], Xiaoman Ma[1], Dasheng Li[4], Jun Chai[5], Dingjun Wang[6], Wenwen Liu[3], Lingbo Lin[3], Jiangfen Wu[2], Chen Xia[2], Zhongfa Zhang[1*]

Manuscript tracking number: SREP-20-02072A

sFig. 1

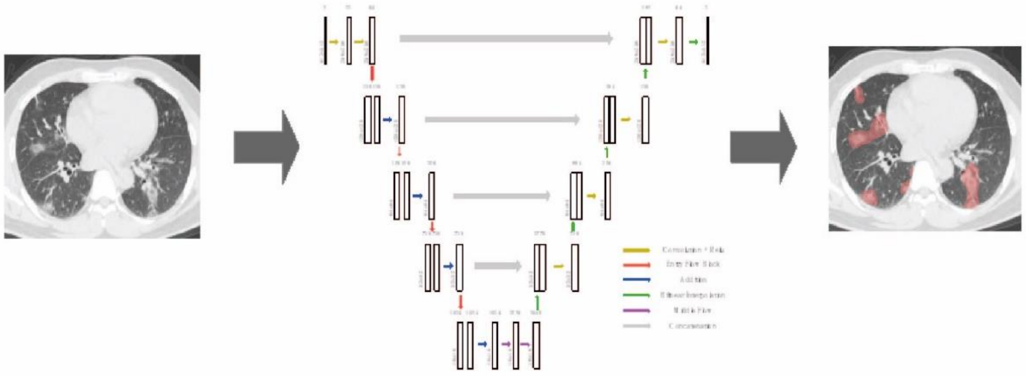

sFig. 1. Architecture of U-Net for infected lesion segmentation. A total of 507 CT scans from suspected COVID-19 patients in Wuhan area constituted the training dataset. Coarse annotation was performed by experienced radiologists, in which multifocal small patchy shadowing, ground-glass opacities, and consolidations were selectively annotated on CT images with major lesions. In subsequent, 7359 slices were utilized to train the DL segmentation algorithm.

sFig.2a

ROC curve

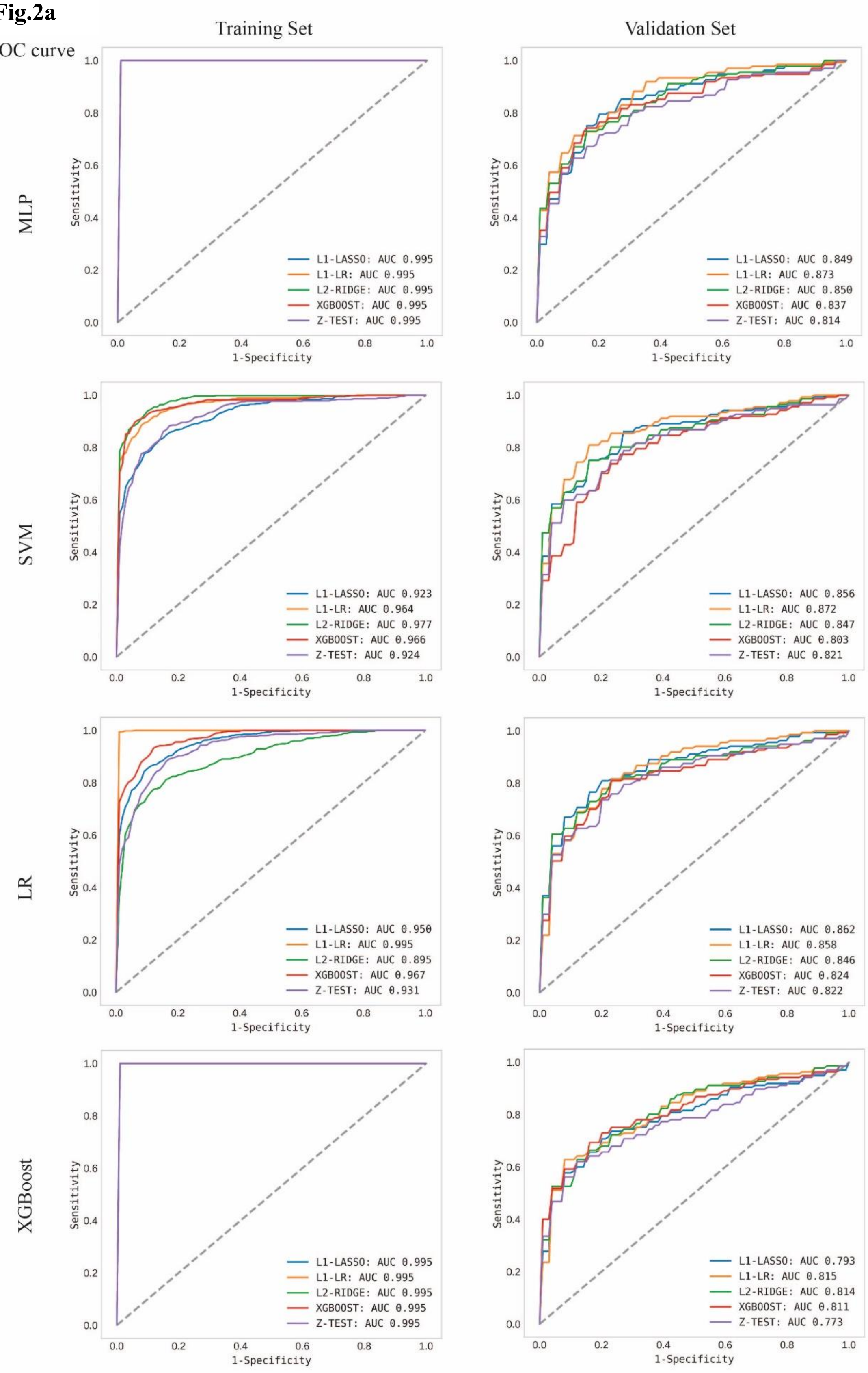

sFig.2b

PR curve

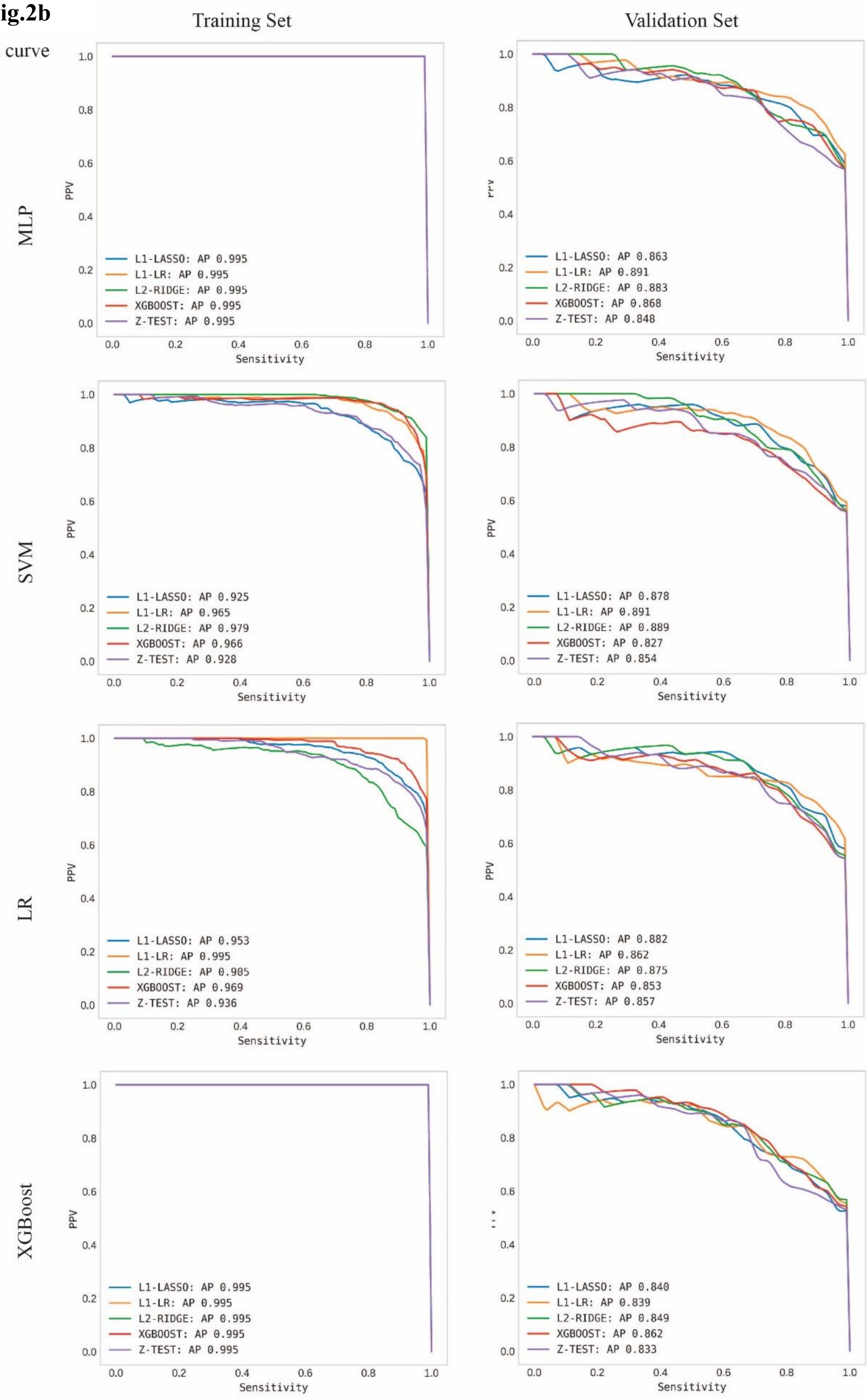

sFig.2. Effectiveness of different radiomic features selection methods. In order to find out the optimal feature selection approach for our study, five representative methods were utilized for feature selection, including L1 regularized least absolute shrinkage and selection operator (L1-LASSO), L1 regularized logistic regression (L1-LR), L1 regularized ridge regression (L2-Ridge), eXtreme gradient boosting (XGBoost), and Z-test. By analyzing the ROC curves (a) and PR curves (b) on the training and validation sets, the performance of corresponding developed models is evaluated to verify and compare the effectiveness of different feature selection methods.

sFigure 3

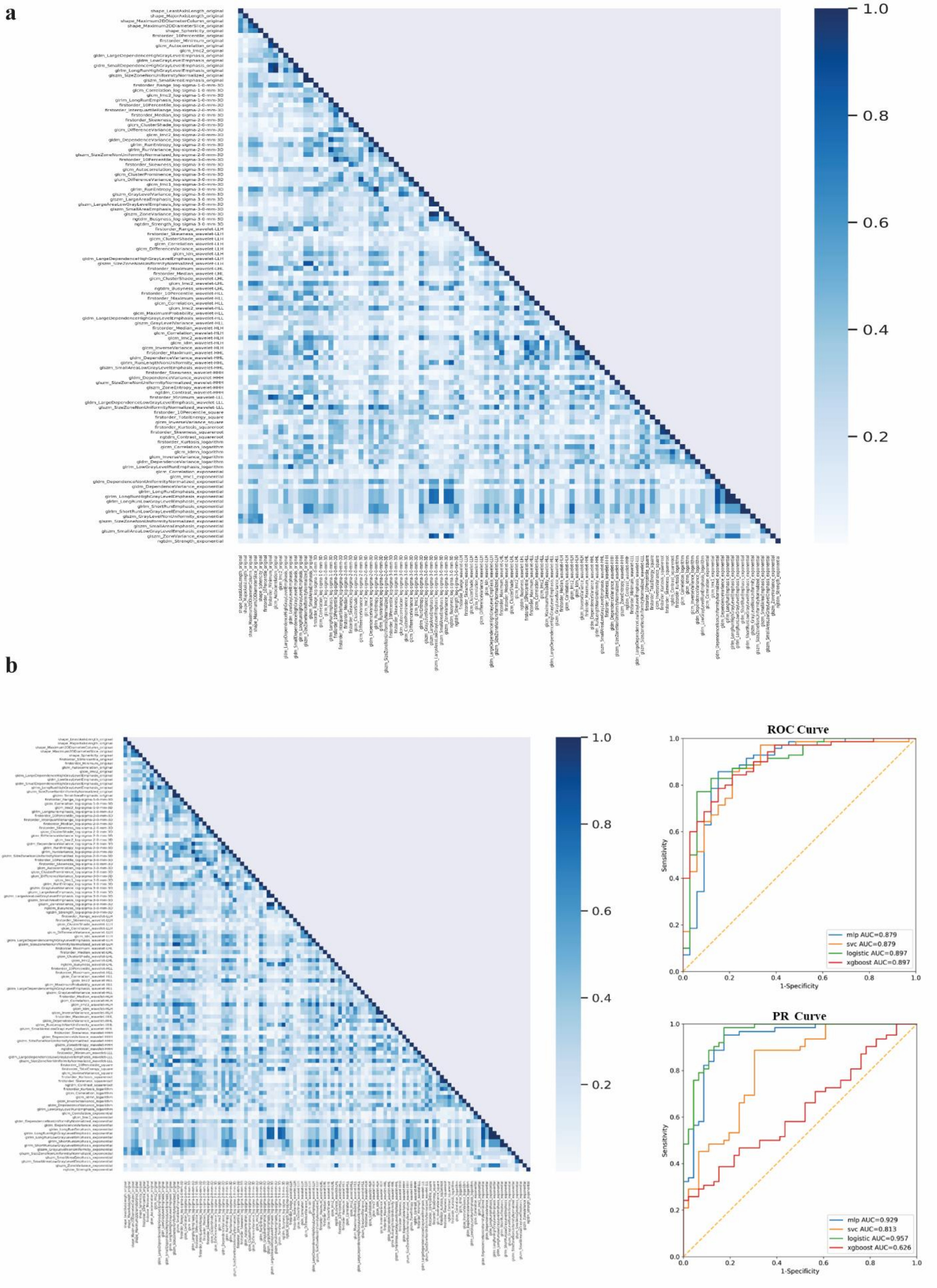
a
shape_LeastAxisLength_original
shape_MajorAxisLength_original
shape_Maximum2DDiameterColumn_original
shape_Maximum2DDiameterSlice_original
shape_Sphericity_original
firstorder_10Percentile_original
firstorder_Minimum_original
glcm_Autocorrelation_original
glcm_Imc2_original
gldm_LargeDependenceHighGrayLevelEmphasis_original
gldm_LowGrayLevelEmphasis_original
gldm_SmallDependenceHighGrayLevelEmphasis_original
glrlm_LongRunHighGrayLevelEmphasis_original
glszm_SizeZoneNonUniformityNormalized_original
glszm_SmallAreaEmphasis_original
firstorder_Range_log-sigma-1-0-mm-3D
glcm_Correlation_log-sigma-1-0-mm-3D
glcm_Imc2_log-sigma-1-0-mm-3D
glrlm_LongRunEmphasis_log-sigma-1-0-mm-3D
firstorder_10Percentile_log-sigma-2-0-mm-3D
firstorder_InterquartileRange_log-sigma-2-0-mm-3D
firstorder_Median_log-sigma-2-0-mm-3D
firstorder_Skewness_log-sigma-2-0-mm-3D
glcm_ClusterShade_log-sigma-2-0-mm-3D
glcm_DifferenceVariance_log-sigma-2-0-mm-3D
glcm_Imc2_log-sigma-2-0-mm-3D
gldm_DependenceVariance_log-sigma-2-0-mm-3D
glrlm_RunEntropy_log-sigma-2-0-mm-3D
glrlm_RunVariance_log-sigma-2-0-mm-3D
glszm_SizeZoneNonUniformityNormalized_log-sigma-2-0-mm-3D
firstorder_10Percentile_log-sigma-3-0-mm-3D
firstorder_Skewness_log-sigma-3-0-mm-3D
glcm_Autocorrelation_log-sigma-3-0-mm-3D
glcm_ClusterProminence_log-sigma-3-0-mm-3D
glcm_DifferenceVariance_log-sigma-3-0-mm-3D
glcm_Imc1_log-sigma-3-0-mm-3D
glrlm_RunEntropy_log-sigma-3-0-mm-3D
glszm_GrayLevelVariance_log-sigma-3-0-mm-3D
glszm_LargeAreaEmphasis_log-sigma-3-0-mm-3D
glszm_LargeAreaLowGrayLevelEmphasis_log-sigma-3-0-mm-3D
glszm_SmallAreaEmphasis_log-sigma-3-0-mm-3D
glszm_ZoneVariance_log-sigma-3-0-mm-3D
ngtdm_Busyness_log-sigma-3-0-mm-3D
ngtdm_Strength_log-sigma-3-0-mm-3D
firstorder_Range_wavelet-LLH
firstorder_Skewness_wavelet-LLH
glcm_ClusterShade_wavelet-LLH
glcm_Correlation_wavelet-LLH
glcm_DifferenceVariance_wavelet-LLH
glcm_Idn_wavelet-LLH
gldm_LargeDependenceHighGrayLevelEmphasis_wavelet-LLH
glszm_SizeZoneNonUniformityNormalized_wavelet-LLH
firstorder_Maximum_wavelet-LHL
firstorder_Median_wavelet-LHL
glcm_ClusterShade_wavelet-LHL
glcm_Imc2_wavelet-LHL
ngtdm_Busyness_wavelet-LHL
firstorder_10Percentile_wavelet-HLL
firstorder_Maximum_wavelet-HLL
glcm_Correlation_wavelet-HLL
glcm_Imc2_wavelet-HLL
glcm_MaximumProbability_wavelet-HLL
gldm_LargeDependenceHighGrayLevelEmphasis_wavelet-HLL
glszm_GrayLevelVariance_wavelet-HLL
firstorder_Median_wavelet-HLH
glcm_Correlation_wavelet-HLH
glcm_Imc2_wavelet-HLH
glcm_Idm_wavelet-HLH
glcm_InverseVariance_wavelet-HLH
firstorder_Maximum_wavelet-HHL
gldm_DependenceVariance_wavelet-HHL
glrlm_RunLengthNonUniformity_wavelet-HHL
glszm_SmallAreaLowGrayLevelEmphasis_wavelet-HHL
firstorder_Skewness_wavelet-HHH
gldm_DependenceVariance_wavelet-HHH
glszm_SizeZoneNonUniformityNormalized_wavelet-HHH
glszm_ZoneEntropy_wavelet-HHH
ngtdm_Contrast_wavelet-HHH
firstorder_Minimum_wavelet-LLL
gldm_LargeDependenceLowGrayLevelEmphasis_wavelet-LLL
glszm_SizeZoneNonUniformityNormalized_wavelet-LLL
firstorder_10Percentile_square
firstorder_TotalEnergy_square
glcm_InverseVariance_square
firstorder_Kurtosis_squareroot
firstorder_Skewness_squareroot
ngtdm_Contrast_squareroot
firstorder_Kurtosis_logarithm
glcm_Correlation_logarithm
glcm_Idmn_logarithm
glcm_InverseVariance_logarithm
gldm_DependenceVariance_logarithm
glrlm_LowGrayLevelRunEmphasis_logarithm
glcm_Correlation_exponential
glcm_Imc1_exponential
gldm_DependenceNonUniformityNormalized_exponential
gldm_DependenceVariance_exponential
glrlm_LongRunEmphasis_exponential
glrlm_LongRunHighGrayLevelEmphasis_exponential
glrlm_LongRunLowGrayLevelEmphasis_exponential
glrlm_ShortRunEmphasis_exponential
glrlm_ShortRunLowGrayLevelEmphasis_exponential
glszm_GrayLevelNonUniformity_exponential
glszm_SizeZoneNonUniformityNormalized_exponential
glszm_SmallAreaEmphasis_exponential
glszm_SmallAreaLowGrayLevelEmphasis_exponential
glszm_ZoneVariance_exponential
ngtdm_Strength_exponential
1.0
0.8
0.6
0.4
0.2
b
1.0
0.8
0.6
0.4
0.2
ROC Curve
Sensitivity
1-Specificity
0.0
0.2
0.4
0.6
0.8
1.0
mlp AUC=0.879
svc AUC=0.879
logistic AUC=0.897
xgboost AUC=0.897
PR Curve
Sensitivity
1-Specificity
0.0
0.2
0.4
0.6
0.8
1.0
mlp AUC=0.929
svc AUC=0.813
logistic AUC=0.957
xgboost AUC=0.626

sFigure 3

c

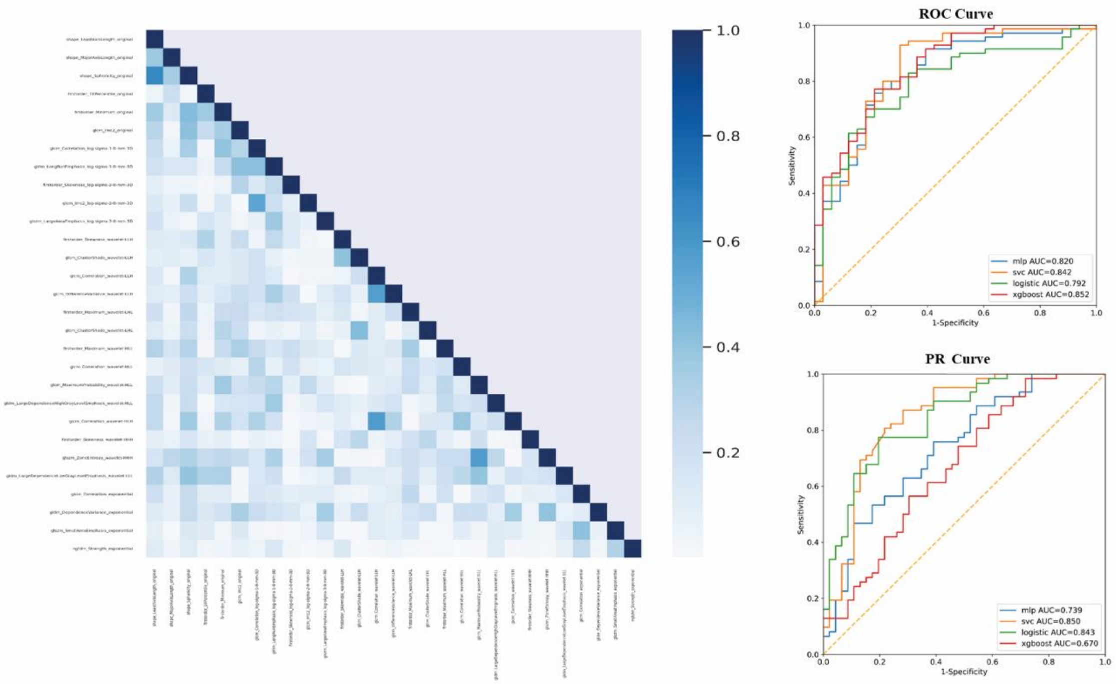

sFig.3. Redundancy analysis for selected radiomics features. Pearson Correlation Coefficient (PCC) among the 108 selected features were calculated. All features, features with PPC < 0.8 and 0.5 constituted three feature sets which were further applied to train the machine learning models. Correlation heat-maps for different feature sets were displayed separately in panel a (108 features), panel b (features with PPC < 0.8), and panel c (features with PPC < 0.5). Model performance was then evaluated in terms of ROC curves and PR curves to examine the feature redundancy (b and c).

sFig.4

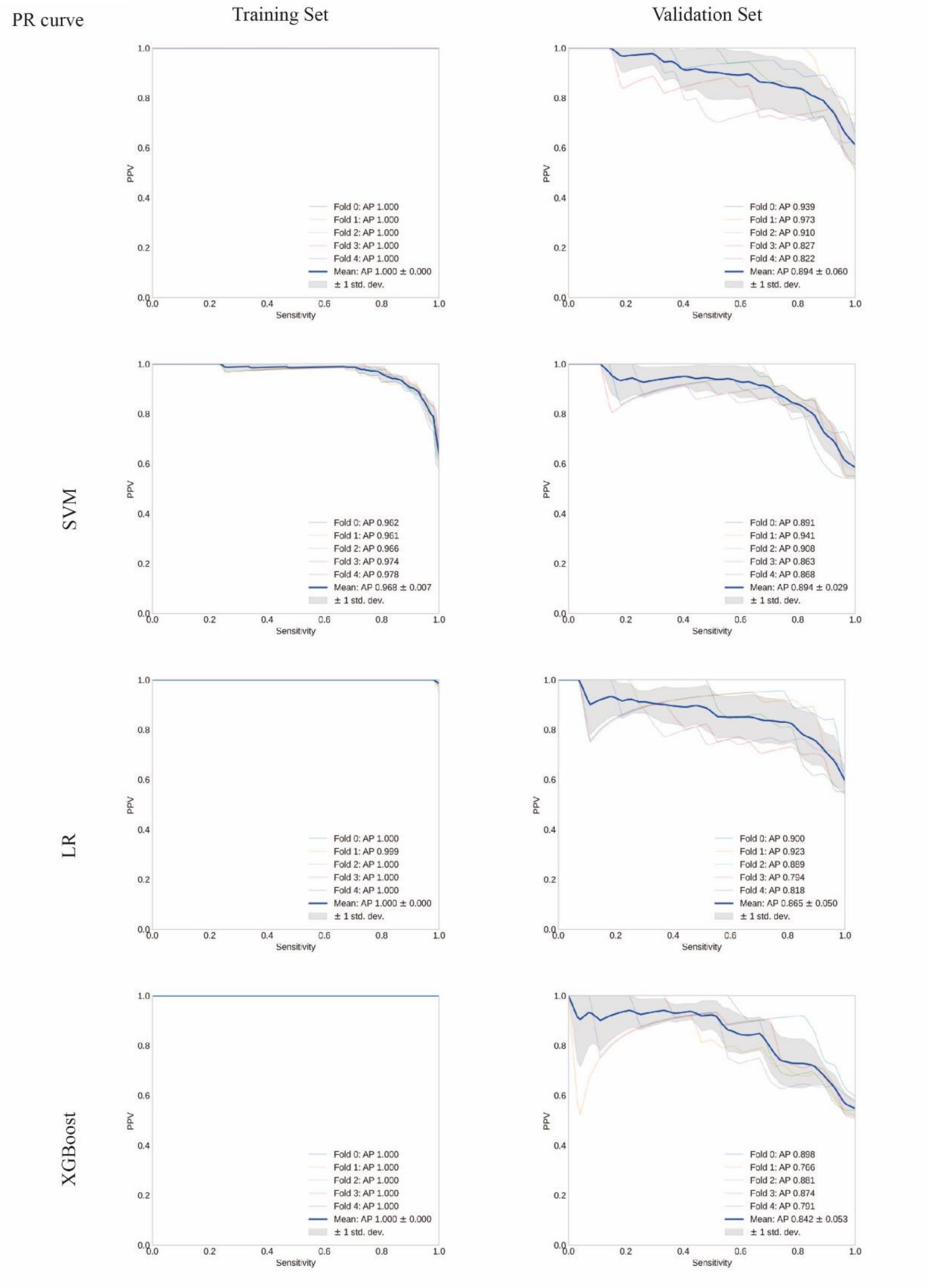

sFig.4. PR curve analyses of ML models on training and validation sets. To evaluate the performance of these ML models, PR curves were also analyzed along with ROC curves on

training and validation sets. Similarly, all ML models but SVM achieved PR-AUC of 1.000 on training set while MLP and SVM displayed a better performance on the validation set.

sFig.5

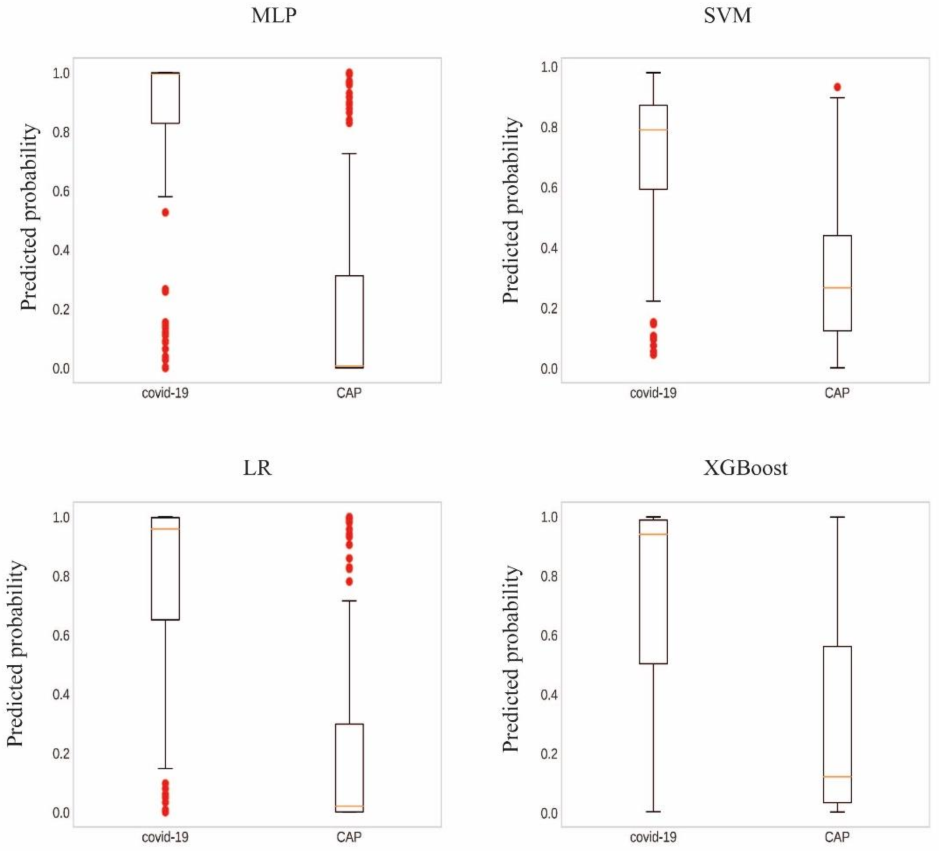

sFig.5. Predictive probabilities of COVID-19 by ML models. Predicted probabilities for COVID-19 and CAP (non-COVID-19) were quite differently distributed. A diagnostic threshold of 0.5 could well discriminate between these two classes.